

# G.S.M.: a Grating Scale Monitor for atmospheric turbulence measurements.

## I. The instrument and first results of angle of arrival measurements

F. Martin<sup>1</sup>, A. Tokovinin, A. Agabi<sup>1</sup>, J. Borgnino<sup>1</sup> and A. Ziad<sup>1</sup>

<sup>1</sup> Département d'Astrophysique, U.R.A. 709 du C.N.R.S., Université de Nice-Sophia Antipolis, Parc Valrose, 06108 Nice Cedex 2, France

<sup>2</sup> Sternberg Astronomical Institute, Universitetsky prosp.13, 119899, Moscow, Russia

Received February 23; accepted May 20, 1994

**Abstract.** — A better understanding of the behavior of wavefronts perturbed by the atmospheric turbulence is vital for the progress in the High Angular Resolution (H.A.R) observing techniques, namely long baseline interferometry and adaptive optics. A new instrument called G.S.M. was built for the study of spatial and temporal properties of wavefronts by means of angle of arrival fluctuation measurements in two (or more) spatially separated points. The Fried parameter  $r_0$ , the wavefront outer scale  $L_0$  and the speckle lifetime  $\tau$  can be deduced from these data. In the first part of this paper the instrument itself is described. It is based on the modulation of a stellar image formed in a small telescope by a Ronchi grating together with a fast scanning mirror. High sampling rate (up to 5 ms), high precision (rms photon noise 0.08'' on  $\alpha$  UMi) and the possibility to have long uninterrupted data sequence are achieved. Examples of the first results include  $r_0$  and  $\tau$  estimates.

**Key words:** atmospheric effects — turbulence — site testing — technique: interferometric — instrumentation: miscellaneous

### 1. Introduction

Ground-based astronomical observations are known to be severely limited by the atmospheric turbulence. Within the usual theoretical framework, the size of a long-exposure image in a large telescope can be characterized by a single turbulence parameter -the Fried parameter  $r_0$  called also coherence radius. Various instruments have been developed for its measurement. With the advent of new High Angular Resolution (H.A.R) observing techniques, interferometry and adaptive optics, a better knowledge of atmospheric turbulence is required. A single parameter  $r_0$  is no longer sufficient, because the performance of H.A.R methods depends also on temporal, spatial and spatio-angular coherence properties of wavefronts perturbed by the terrestrial atmosphere. These parameters are discussed in some detail below.

In response to a need for the measurements of all turbulence parameters relevant to H.A.R observing techniques, we started a program for the development of a seeing monitor of a new type that would be capable of measuring not only the Fried parameter  $r_0$  but also the global outer scale of turbulence and its characteristic time  $\tau$ . Our effort is based on a large previous experience of at-

mospheric turbulence measurements accumulated at our laboratories. In this paper we describe our basic instrument and its first results on measurements of  $r_0$  and  $\tau$ . The second paper will deal with the method of turbulence outer scale measurements (Borgnino et al. 1992) and will contain our estimates of this parameter.

Our approach consists in measuring the angle of arrival fluctuations at several (at least 2) points on the wavefront with a sufficient time resolution. The image position is measured using Ronchi grating placed in the focal plane of a small telescope, hence the device was baptized Grating Scale Monitor (G.S.M). The final results are obtained by suitable processing of these data. A short review of relevant parameters and existing techniques of their measurement is presented in the next section.

### 2. Atmospheric parameters relevant to high angular resolution observing

#### 2.1. Fried's coherence length

It can be defined as the diameter of a wavefront area over which the rms phase variations due to atmosphere are equal to 1 rad. A more strict definition relates  $r_0$  to the

phase structure function  $D_\phi(\mathbf{r})$  (Tatarski 1961; Roddier 1981) which under Kolmogorov law must be of the form:

$$D_\phi(\mathbf{r}) = 6.88 \left( \frac{r}{r_o} \right)^{5/3}, \quad (1)$$

where  $r = |\mathbf{r}|$  denote the modulus of the spatial shift. The relation of  $r_o$  to the refractive index structure coefficient  $C_N^2(h)$  and wavelength  $\lambda$  for observations at zenith (Roddier 1981) is:

$$r_o^{-5/3} = 0.423 \left( \frac{2\pi}{\lambda} \right)^2 \int_0^\infty dh C_N^2(h), \quad (2)$$

where  $h$  is the altitude of the layers. The angle of arrival fluctuations measured at the focus of a small telescope of diameter  $D$  are also directly related to  $r_o$  (Fried 1966; 1975; Tatarski 1971):

$$\sigma_D^2 \cong 0.179 \lambda^2 r_o^{-5/3} D^{-1/3}, \quad (3)$$

where  $\sigma_D^2$  is the angular dispersion in one direction, expressed in radians. A number of devices has been constructed which employ expression (3) to estimate  $r_o$  from  $\sigma_D^2$ , and G.S.M. can also be used for this purpose (see Sect. 4.2). Yet another technique for measurements of  $r_o$  consists in direct evaluation of the atmospheric coherence function by an interferometer attached to a telescope with a suitably large aperture ( $D > r_o$ ) (Roddier C. 1976). Both interferometer and  $\sigma_D^2$  monitors are sensitive to telescope pointing errors that can hardly be distinguished from atmospheric fluctuations. This consideration has led to the development of Differential Image Motion Monitors (DIMM), first pioneered by Stock & Keller (1960) and nowadays used extensively in site testing campaigns (e.g. Sarazin 1986). In this case the difference of angle of arrival fluctuations as observed using two small circular apertures of diameter  $D$  separated by a baseline  $d$  is measured. Its dispersion  $\sigma_D^2(d)$  (Sarazin & Roddier 1990) is related to  $r_o$  by:

$$\sigma_D^2(d) \cong 2\lambda^2 r_o^{-5/3} (0.179 D^{-1/3} - \alpha d^{-1/3}), \quad (4)$$

where  $\alpha = 0.0968$  for longitudinal motion (parallel to the baseline) and  $\alpha = 0.145$  for transverse motion. The current version of G.S.M. was also tested in a DIMM configuration (see Sect. 4.2).

## 2.2. Wavefront outer scale $\mathcal{L}_0$

In the turbulence theory the outer scale  $L_0$  is considered as a parameter that defines the greatest size of eddies. The phase structure function of a wavefront passed through a single turbulent layer saturates at  $r \geq L_0$ . So the Kolmogorov law (1) is valid only in the so-called inertial range, for  $r \ll L_0$ . Various expressions for  $D_\phi(\mathbf{r})$  that take into account its saturation at larger  $r$  can be found in the literature (Lutomirski 1971). In reality the

light passes through many turbulent layers of different strengths and different  $L_0$ . Their combined effects on the wavefront is characterized by a spatial coherence outer scale of the wavefront (Borgnino 1990) called also *wavefront outer scale*  $\mathcal{L}_0$ . It is related to the geophysical outer scale of different turbulent layers  $L_0(h)$  by a weighting formula:

$$\mathcal{L}_0^{-1/3} = \frac{\int_0^\infty dh L_0^{-1/3}(h) C_N^2(h)}{\int_0^\infty dh C_N^2(h)}. \quad (5)$$

The parameter  $\mathcal{L}_0$  is relevant to the operation of long-baseline interferometers because the atmospheric optical path length variations depend on it. Thus it is very desirable to have a  $\mathcal{L}_0$  monitor near the interferometers. Conversely,  $\mathcal{L}_0$  can be measured directly with an interferometer. Such estimates have been published by Mariotti et al. (1984), Colavita et al. (1987), and Busher et al. (1991). The optical path length in an interferometer depends not only on the atmospheric phase differences but also on the instrument itself (thermal drifts, mechanical errors, etc.). So direct interferometric measurements of  $\mathcal{L}_0$  is not a very clear method, and also a very expensive one. A less direct but more robust approach is the comparison of angle of arrival measured at different parts of the wavefront. Several attempts of this kind were made with wavefront sampling on a telescope aperture (Tallon 1989; Rousset et al. 1991; Ziad et al. 1993). The extension of this technique to greater baselines is the main task of G.S.M. We must mention here an early attempt of this kind (Ataev et al. 1982).

## 2.3. Characteristic time $\tau$

The temporal evolution of atmospheric disturbances places severe limit on the exposure time of an interferometer or an adaptive optics wavefront sensor and hence limits their sensitivity. If wind and turbulence altitude profiles  $\mathbf{v}(h)$  and  $C_N^2(h)$  were known,  $\tau$  could be evaluated theoretically (Roddier & Léna 1984a; Lopez 1992). The corresponding expressions differ for different observing techniques. For speckle interferometry  $\tau = 0.36 r_o / \Delta v$  where  $\Delta v$  is a measure of  $\mathbf{v}(h)$  dispersion with a suitable  $C_N^2(h)$  weighting (Roddier et al. 1982). For small-aperture interferometry and adaptive optics the characteristic time is estimated as  $\tau = 0.31 r_o / v^*$ , where  $v^*$  is some average wind speed. In typical conditions both expressions for  $\tau$  lead to similar estimates. Unfortunately they cannot be used in most cases because wind and  $C_N^2(h)$  height profiles are not known. Direct optical measurements of  $\tau$  are thus of great value. We shall not review here the numerous estimates of speckle lifetime made at the telescopes with interferometric instruments. G.S.M. data consisting of the time series of angle of arrival measurements at two points on the wavefront can be used to estimate the average wind speed and hence  $\tau$ .

## 2.4. Isoplanatic angle and spectral bandwidth

For the sake of completeness we mention here two other atmospheric parameters relevant to H.A.R observing. The isoplanatic angle defines the usable field of view in stellar interferometry and depends directly on  $C_N^2(h)$  profile. The G.S.M. is not easily applicable to such measurements. The  $C_N^2(h)$  profile can be measured by in situ soundings or using SCIDAR (i.e Scintillation Detection and Ranging) (Vernin & Azouit 1983). The spectral bandwidth of an interferometer is also related to atmospheric corrugations of the wavefront (Roddier & Léna 1984b). Given  $r_o$  and  $\mathcal{L}_0$  it can be calculated and hence no special monitor is required for its measurement.

## 3. Description of the instrument

### 3.1. General features

The review of the measurement techniques presented above clearly indicates that an instrument capable of measuring angle of arrival fluctuations in two sufficiently separated parts of a wavefront can be employed for the estimation of major atmospheric parameters relevant to the H.A.R techniques:  $r_o$ ,  $\mathcal{L}_0$  and  $\tau$ . Our desire to use the instrument for site testing and to avoid possible effects of telescope dome has lead to a completely autonomous device. A major consideration is the need to have long time series of angle of arrival measurements that would be free of any guiding errors. We use the Polar star ( $\alpha$  UMi) as light source and observe it with fixed telescopes. A relatively wide field of view ( $20'$ ) permits uninterrupted data acquisition during 40 minutes as the star drifts through the field, due to its diurnal motion. Finally, the temporal spectrum of angle of arrival fluctuations observed with small apertures extends to several tens of Hertz. A temporal resolution of 5 ms is adequate to sample frequencies up to 100 Hz. This data rate is not very high by modern standards but it is incompatible with real-time image processing. This is why we have chosen not to register stellar images by a panoramic detector but rather to measure their coordinate in one direction directly with the help of a grating. A Ronchi grating is placed in the focal plane of the telescope. Its period is greater than the size of stellar image so that the transmitted light depends on the image position. This image is rapidly moved back and forth over one grating period in order to measure its instantaneous position. A similar technique named Phase-Measurement Interferometry is used to measure the phase of interference fringes (Creath 1988). Of course the image position is measured only within a fraction of grating period. However an uninterrupted data sequence is sufficient to reconstruct the image displacement over several grating periods by removing the discontinuities corresponding to the passage from one period to the next. The use of a focal plane grating in combination with rapid modulation has for evident advantage that the displacement of

the stellar image in one direction can be measured with high precision over a large field of view in real time. The instrument is not very complex, but the difficulties consist in ensuring precise linear modulation of image with a well controlled amplitude, and in eliminating other sources of errors. The solutions proposed to overcome these problems are addressed in the following sub-sections.

### 3.2. Image modulation

In our instrument the rapid scanning of the stellar image over the grating is made by the tilts of a plane mirror actuated by a galvanometric coil. The formidable problem of achieving high linearity and speed is solved in an unusual way. Instead of supplying a linear voltage to the coil and making the mirror to follow it as close as possible, we use natural inertia of the mechanical system that ensures a perfectly linear motion in the absence of any external forces. The positive and negative periodic current pulses are injected into the coil (Fig. 1b). During the pulses the angular velocity of the coil changes its sign, and between the pulses the coil continues to turn with constant velocity (Fig. 1a). The angle of the moving mirror as a function of time is proportional to the integral of the current pulses. In fact the integrating properties of our mechanical system are not ideal since the coil with mirror is not completely free from external forces. The most important of these is the elastic force of the suspension. If the driving pulses vanish, the mirror would not turn indefinitely but would rather oscillate with its natural frequency  $f_r$ . It is easily shown that a 1% linearity is ensured if  $f/f_r > 6.4$ , where  $f$  is the modulation frequency. In our case  $f_r = 30$  Hz and  $f=200$  Hz. Our experience has shown that the performance of such modulator is indeed very high. Modulation frequency of 1 kHz can be easily attained and it is in practice limited by the data acquisition rate rather than by the modulator itself. The nice feature of this approach is also the ease of the synchronization of modulation with the data acquisition and the possibility to have several perfectly synchronized modulators. This last property will be used in the future to operate simultaneously several angle of arrival sensors.

### 3.3. Data acquisition

The custom-made card for an IBM PC-AT compatible computer controls the data acquisition and the modulating mirror. The computer clock is used as time base to generate the pulses supplied to the mirror. Photon pulses coming from photomultipliers are counted by 16 bit counters. Each modulation period is divided into 10 intervals by the pulses of frequency  $f_0 = 10f$  (Fig. 1d). These pulses generate computer interrupts to read counters and to accumulate the counts into four channels *A*, *B*, *C*, *D* (Fig. 1c). In the current configuration we set  $f_0 = 2000$  Hz, so that 1 scan takes 5 ms ( $f = 200$  Hz). The calculation

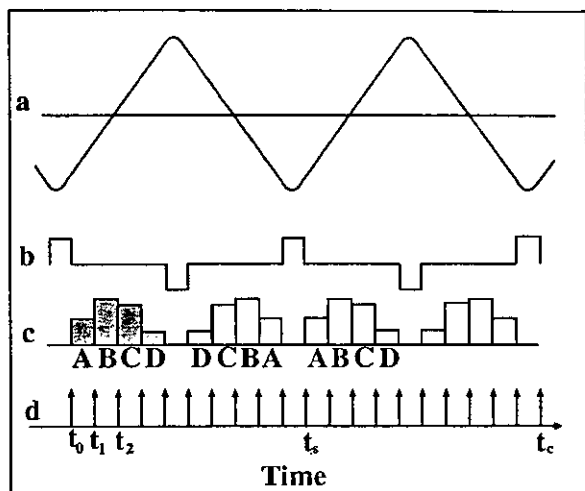


**Fig. 1.** Modulation and acquisition time sequence. The image position as a function of time (a) follows a triangular waveform determined by the current pulses of alternating polarity (b). Each modulation half-period is divided into 4 intervals and the signals *A*, *B*, *C*, *D* are obtained by integration of photon counts over these intervals (c). The counters are read at the moments  $t_0$ ,  $t_1$ ,  $t_2$ , ... marked by small arrows (d). One modulation period ( $t_0 - t_s$ ) is called *scan* and several scans ( $t_0 - t_c$ ) are accumulated in a *cycle* of acquisition to provide the signals *A*, *B*, *C*, *D* used for the calculation of image position

of the image position from *A*, *B*, *C*, *D* can be made by several techniques as reviewed by Creath (1988). It gives the stellar image displacement on the Ronchi grating. This displacement can be monitored in real time.

### 3.4. Optical scheme

Our choice of the optical scheme was motivated by the desire to measure simultaneously the image motion in two beams with one telescope. The beams coming from the stellar source are deflected by two plane mirrors and enter the Schmidt-Cassegrain telescope (Celestron 8) as shown in Fig. 2a. The size of each beam is limited by a 6×6 cm mask and the beam separation is  $d = 14$  cm. The baseline can be changed by changing the separation of plane mirrors. Alternatively the small mirror can be removed and both beams are then reflected by a large mirror. In this configuration G.S.M. is equivalent to a DIMM image quality monitor with a fixed 14 cm baseline. The field lens 1 (Fig. 2b) is located near the focal plane of the telescope and forms the image of its entrance pupil on the pupil mask 4 with two rectangular openings that define the size and separation of incoming beams. After collimating lens 2 the beams are parallel again. They are reflected by plane modulating mirror 5 and the camera lens 6 reforms stellar images on the Ronchi grating 7. The widths of its transparent and opaque parts are equal and the grating period is 40 microns. The Fabry lens 8 reimages the pupil mask

in the vicinity of separating prism 9 with aluminized sides. The modulated light corresponding to two channels is detected by photomultipliers 10 and 11.

The period of Ronchi grating as projected onto the sky has been chosen to be around 5 arcsec in a first step and is now about 8 arcsec. This choice results from a compromise between the desire to increase the measurement precision and the necessity to have a high contrast of light modulation.

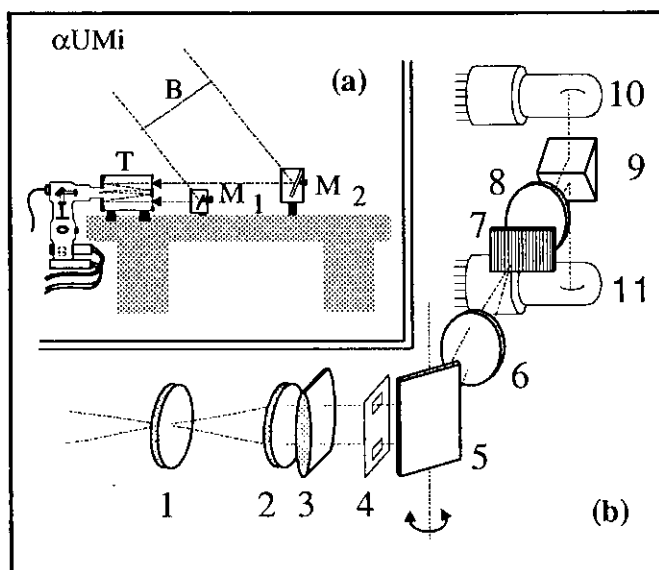


**Fig. 2.** The optical scheme of G.S.M.-Grating Scale Monitor. The part (a) shows how input beams coming from the stellar source are directed into the telescope *T* by two mirrors  $M_1$  and  $M_2$ . (b) Acquisition and detection module (see the text)

### 3.5. Analysis of the precision of measurements

The measured position of the star is affected by errors of different kinds. In this sub-section they are analyzed in turn.

#### 3.5.1. Imperfect modulation

Creath (1988) has shown that the misalignment of the modulation amplitude or the modulation non-linearity of 10% cause the errors on calculated positions of approximately 0.01 period. The magnitude of these errors depends on the procedure used to calculate positions. The errors are periodic with double grating frequency. The effect of detector non-linearity was also analyzed, leading to similar conclusions. In our case the non-sinusoidal character of light modulation can also cause periodic position errors with quadruple grating frequency. The linearity of modulation is more or less ensured by the concept of the modulator and a special procedure has been performed to adjust or check the modulation amplitude with great confidence. The final control of modulation errors was made

in the laboratory by comparison of the position of an artificial star on the Ronchi grating with the value measured by our instrument. The results are presented in Fig. 3 which displays the residuals between measured positions and the linear fit to the data. The errors do not exceed 0.005 grating period. Thus the combined influence of the modulation errors mentioned above is small.

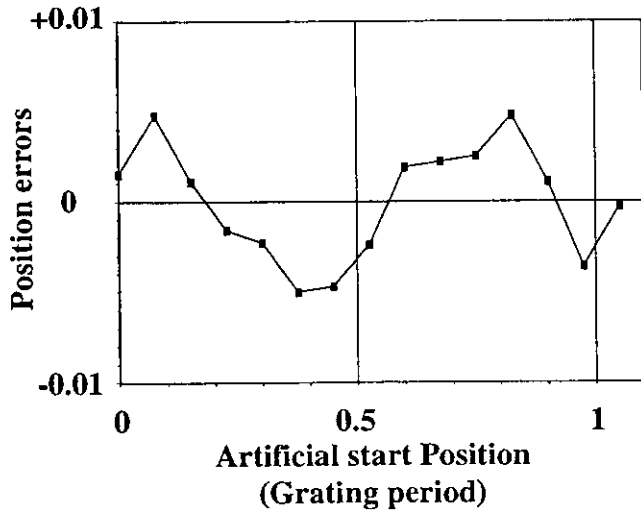


**Fig. 3.** Test for the position measuring errors due to imperfect modulation. Position errors are differences (in grating period) between measured position of the artificial star and a linear fit

### 3.5.2. Photon noise

The limited light flux of the stellar source with the associated statistical noise is the main factor that defines the measurement precision. A simple derivation based on the Poisson law and the phase calculation formula leads to the expression for  $\sigma_p$  (the rms position fluctuations in the units of grating period):

$$\sigma_p = \frac{1}{8\gamma\sqrt{N}}, \quad (6)$$

where  $N$  is the average number of photons per acquisition (i.e. the average of  $A$ ,  $B$ ,  $C$ ,  $D$ ) and

$$\gamma^2 = \frac{\pi^2 (A - C)^2 + (B - D)^2}{2 (A + B + C + D)^2} - \frac{\pi^2}{8N} \quad (7)$$

is the square of the modulation contrast (the measured contrast is a factor  $\text{sinc}(0.25)=0.9$  less than  $\gamma$  because the signals are integrated over  $1/4$  period). This contrast estimate is unbiased because the photon noise contribution is taken into account by the second term. The validity of these formulae was proven by direct measurements of position fluctuations in stable laboratory conditions. With the star  $\alpha$  UMi as a light source and in good transparency conditions we have  $N = 400$  (at 20 ms time resolution – 4 scans per cycle) and  $\gamma = 0.6$  which gives photon error of

the order of 0.01 grating period or  $0.08''$ . It is much less than the atmospheric fluctuations.

### 3.5.3. Scintillation noise

The stellar flux received by a small telescope is known to fluctuate due to scintillation (Roddier 1981). The effect of this flux modulation must be considered. Indeed, the measurements show that the dispersion of the signals  $A$ ,  $B$ ,  $C$ ,  $D$  is typically 3 times more than their photon dispersion  $N$ . However most of the flux changes occur on a time scale greater than the scan time and hence do not influence position measurements. To measure scintillation, a cylindrical lens is used (Fig. 2b) which disperses stellar image along grating ruling. Hence, when the grating is turned the modulation is absent and the rapid fluctuations of the flux only remains which can be measured directly. Our measurements indicate that the influence of rapid scintillation is negligible in comparison with the photon noise (about 5 or 6%).

## 4. Results

### 4.1. Measured signals

The first measurements with G.S.M instrument were obtained at Calern Observatory (Observatoire de la Côte d'Azur – O.C.A) in October and December 1993. The angle of arrival fluctuations are simultaneously recorded on the two acquisition channels. Figure 4a shows an example of image motion in one channel as registered on October 20th with a baseline of 14 cm. Time resolution was 20 ms, and the duration of acquisition 300 s.

One can see in Fig. 4a the slow drift due to the diurnal motion of the star. This drift was approximated by a parabola and subtracted from the data to leave atmospheric angle of arrival fluctuations. The comparison of the fitted slope with its theoretical value is used to find the angular period of the Ronchi grating. Such a calibration based on 21 data sequences obtained in October leads to the grating period of  $5.16'' \pm 0.063$ . The angles of arrival obtained after the subtraction of diurnal motion are depicted in Fig. 4b. The rms photon noise estimated by formula (6) is  $0.07''$ , with mean contrast of 47%. This noise contribution was subtracted quadratically in subsequent analysis. Our first data sets frequently presented discontinuities of 1 grating period as shown in Fig. 5a. The plot of corresponding modulation contrast is given in Fig. 5b and shows that these phase jumps occur when the modulation contrast is reduced by small-scale distortions of wavefront. The jumps were observed to occur frequently on periods of poor seeing and were practically absent when the seeing was good. A consequence of this experience the grating period was increased to  $8''$ . It seems to be a good compromise for the typical seeing conditions. The contrast is better and phase jumps are rare. An algorithm was de-

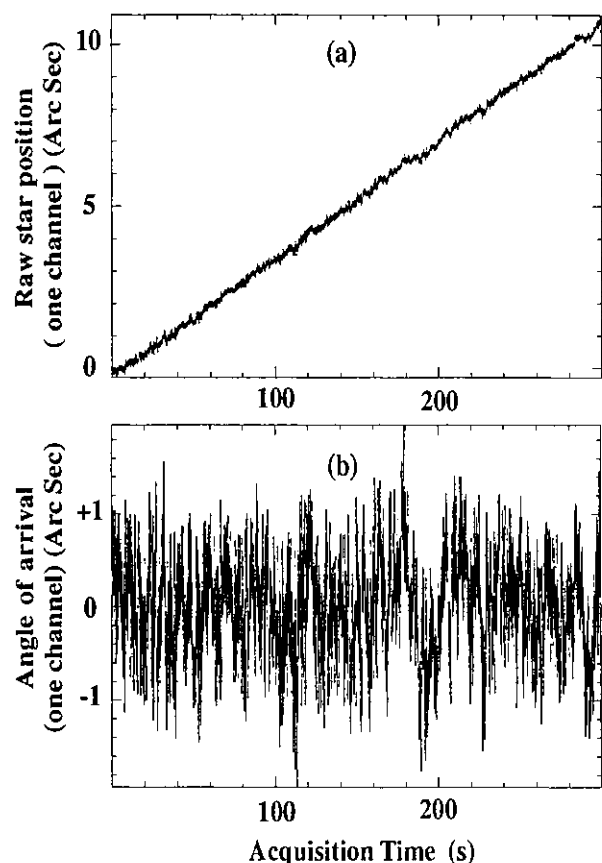


**Fig. 4.** Position of  $\alpha$  UMi image on the Ronchi grating as a function of the time. a) The slow drift of the star superimposed to the angle of arrival fluctuations is seen. b) The angle of arrival only remains when the diurnal motion is subtracted

veloped to detect and correct the phase jumps as shown in Fig. 5c. This algorithm is incorporated in the standard data processing and eventually takes care of the remaining phase jumps.

#### 4.2. Estimation of Fried's parameter $r_o$ from angle of arrival observations

For the evaluation of the Fried parameter  $r_o$ , G.S.M was operated in the DIMM configuration. The values of  $r_o$  were deduced from the one dimensional variance of angle of arrival fluctuations (3) with the size of the pupil  $D = 6$  cm. In fact, the experiment being a dual channel one, the two values  $r_{o1}$  and  $r_{o2}$  were computed from the variance of each channel. An example of typical results is shown in Fig. 6 where the data obtained during 3 periods of observations on the same night are represented. The Fried parameter  $r_{oDIMM}$  was also computed from the variance of differential image motion measured simultaneously with two sub-apertures. The expression (4) was used with  $d = 14$  cm and  $\alpha = 0.145$  because in our experimental configuration G.S.M. was sensitive to the transverse image motion. As can be seen from Fig. 6 the values  $r_{o1}$  and

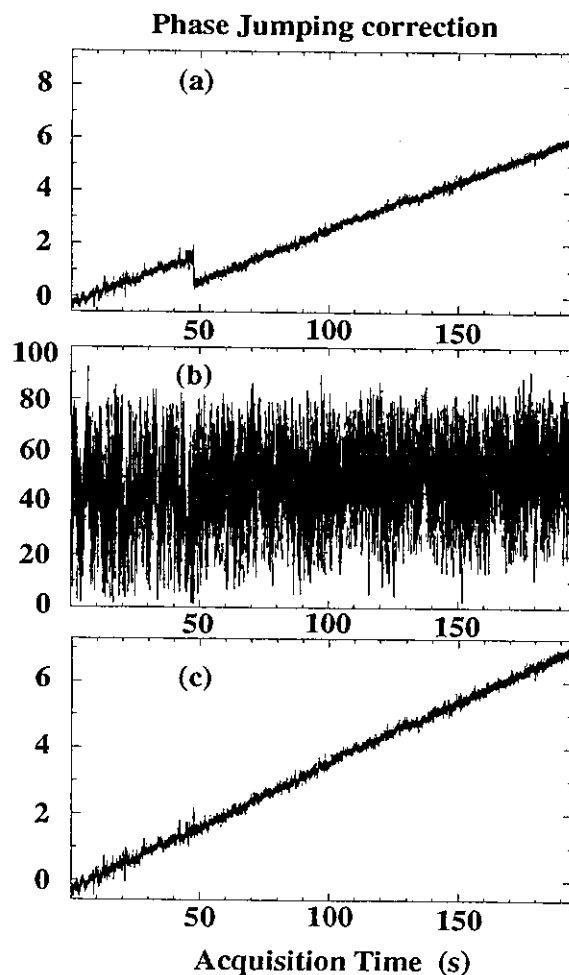


**Fig. 5.** Example of phase jumping. a) Recording of the position of the star affected by a phase jump of one grating period. b) Corresponding contrast (%). c) Recovered position obtained by using appropriate algorithm

$r_{o2}$  computed for the variance method are in very good agreement with the values  $r_{oDIMM}$ . The agreement of the  $r_o$  values obtained in two different ways from our data is an important step in the validation of the measurement and reduction procedure. It indicates clearly the absence of guiding errors and vibrations in the single-channel data, at least down to the level of atmospheric angle of arrival fluctuations.

#### 4.3. Estimation of an average wind speed and speckle life time from temporal cross-spectra

As another example of results deduced from our first measurements on the sky, a temporal cross-spectrum for angle of arrival fluctuations is presented in Fig. 7 with a sampling time of 5 ms, and where the cut-off frequency is 100 Hz. This cross-spectrum is the average of 14 individual cross-spectra computed on successive 41 seconds samples of angle of arrival. Several authors have experimentally

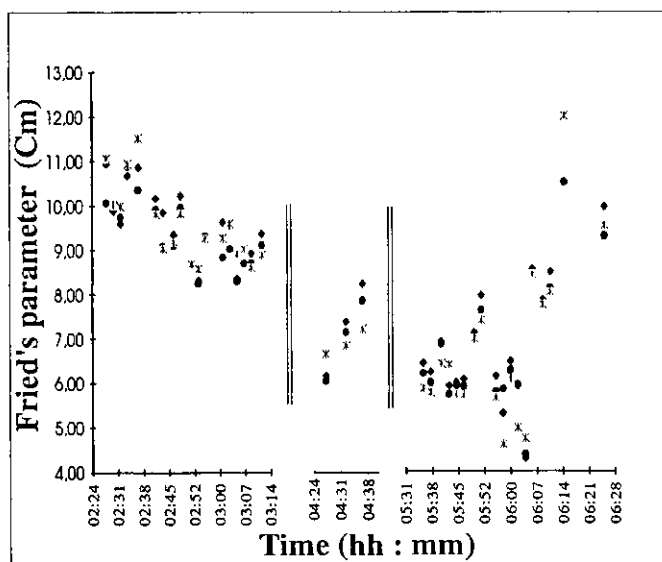


Fig. 6. Comparison of the estimation of Fried's parameter  $r_o$  from a) the variance of angle of arrival:  $r_{o1}$  ( $\bullet$ ) for channel 1 and  $r_{o2}$  ( $\diamond$ ) for channel 2. b) the variance of differential image motion  $r_{oDIMM}$  (\*). For this comparison G.S.M. was operated in DIMM configuration

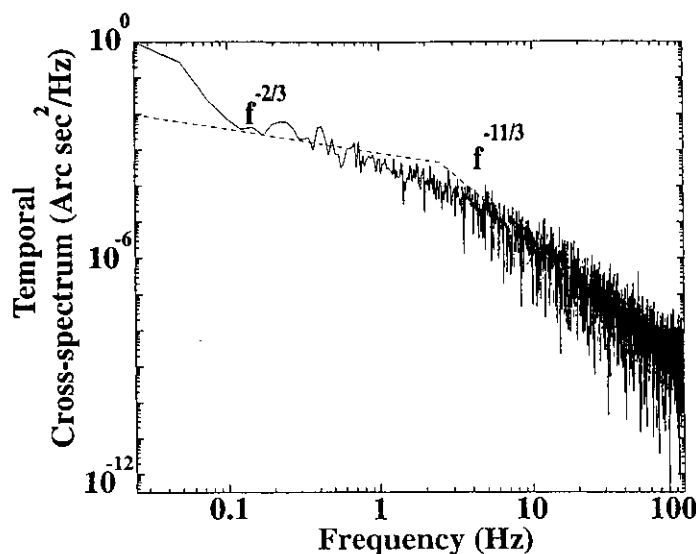


Fig. 7. An example of temporal cross-spectrum of angle of arrival. The sampling rate for data acquisition was 5 ms

proved that the power spectra of the fringe position in an interferometer (Colavita et al. 1987; Buscher et al. 1991) or the power spectra of the atmospheric phase fluctuations (Nightingale & Buscher 1991) show a typical behavior characterized by two regions with different power laws. The behavior is the same for the power spectrum of angle of arrival: this power laws being  $f^{-2/3}$  in the low frequency domain and  $f^{-11/3}$  in the high frequency one (Conan et al. 1992; Ziad et al. 1993). The characteristic frequency  $f_c$  dividing the low-and high-frequency parts of power spec-

trum can be roughly estimated as  $f_c = 0.3v^*/D$  (Tango & Twiss 1980; Conan et al. 1992) if Taylor's frozen turbulence hypothesis is assumed. Here  $v^*$  is the average wind speed which determines the correlation time of the wavefront corrugations (see Sect. 2.3) and  $D$  is the size of the aperture. The modulus of the cross-power spectrum must exhibit similar behavior, but the aperture size  $D$  in the expression for  $f_c$  is to be replaced by the baseline  $d$ . Thus in comparison with the single-channel power spectrum the  $f_c$  is shifted to the lower frequencies and can be measured with much better confidence. An additional advantage of cross-spectrum over power spectrum is to eliminate the high frequency photon noise which is uncorrelated in the two channels.

By fitting a  $f^{-2/3}$  straight line to the low-frequency part of the spectrum and a  $f^{-11/3}$  one to its high frequency region the value of  $f_c = 2.5$  Hz can be roughly estimated from Fig. 7. This value corresponds to an average wind speed of  $v^* = 1.16$  m/s. Taking into account the value of  $r_o = 9$  cm computed for these data a characteristic time  $\tau$  of the order of  $0.31r_o/v^* = 24$  ms is deduced. This coarse interpretation is only given here to indicate the potential of G.S.M experiment in the field of temporal characterization of atmospheric wavefront.

#### 4.4. Discussion

When we decided to develop G.S.M our initial goal was to build a small transportable instrument dedicated not only to the measurement of the spatial coherence outer scale  $\mathcal{L}_0$  but also to the Fried parameter  $r_o$  and to characteristic times of the turbulence. The first step of this program is accomplished, and a two channel calibrated device is now built to measure angle of arrival of the wavefront in two points separated by an adjustable distance. This device used with the star  $\alpha$ UMi as a light source permits to make such measurements with an angular precision of the order of  $0.08''$  and a sampling rate of 5 ms.

Using G.S.M in a first set of experiments in October 1993 at the O.C.A-Calern site has permitted to collect the preliminary data. Processing of these data has given  $r_o$  values from variances and covariances of angle of arrival, and a characteristic time  $\tau$  from the modulus of angle of arrival cross-spectrum. From the phase of the same cross-spectrum it will be possible to estimate another important parameter: the component of the average wind velocity in the direction of the baseline. This is beyond the scope of this paper and a study of the time constants will be undertaken in the future when more data will be available.

Concerning measurements of the outer scale  $\mathcal{L}_0$ , the necessary equipments to make an easy and fast change of the baseline is now built at the O.C.A-Calern site and the measurements have begun. In a near future a second paper will be devoted to the values of  $\mathcal{L}_0$  deduced from G.S.M and to the related theory.

*Acknowledgements.* G.S.M. is operating in the Calern and Mont-Gros sites of Observatoire de la Côte d'Azur (O.C.A.). The authors would like to thank the O.C.A. members for their hospitality and technical help. Thanks go specially to the staff of the optical laboratory for their friendly cooperation. The authors thank Peter Lawson for bringing some useful references to our attention. Financial support for this work comes essentially from INSU (Institut National des Sciences de l'Univers), French M.E.S.R (Ministère de l'Enseignement Supérieur et de la Recherche), and from the France-Russia P.I.C.S (Programme International de Coopération Scientifique).

## References

- Ataev A.Sh., Beslik A.I., Guryanov A.E. et al. 1982, *Astron. Tsikular* 1293, 6
- Borgnino J. 1990, *Appl. Opt.* 29, 1863
- Borgnino J., Martin F., Ziad A. 1992, *Opt. Com.* 91, 267
- Buscher D.F., Armstrong J.T., Mozurkewich D., Denison C.S., Colavita M.M., Shao M. 1991, *High-Resolution Imaging by Interferometry II* (ESO Proc. Garching) 1029
- Colavita M.M., Shao M., Staelin D.H. 1987, *Appl. Opt.* 26, 4106
- Conan J.M., Madec P.Y., Rousset G. 1992, *Real Time and Post-Fact Solar Image Correction*, 13th Sacramento Peak Summer Workshop
- Creath K. 1988, ed. E. Wolf, *Prog. Opt.* 14, 349
- Fried D.L. 1966, *J. Opt. Soc. Am.* 56, 1372
- Fried D.L. 1975, *Radio Sci.* 10, 71
- Lopez B. 1992, *A&A* 253, 635
- Lutomirski R.F., Yura H.T. 1971, *J. Opt. Soc. Am.* 61, 482
- Mariotti J.M., Di Benedetto. G. 1984, *Very Large Telescopes, their Instrumentation and Programs*, Proc. IAU Colloq. 79 (Garching) 257
- Nightingale N.S., Buscher D.F. 1991, *MNRAS* 251, 155
- Roddier C. 1976, *J. Opt. Soc. Am.* 66, 478
- Roddier F. 1981, ed. E. Wolf, *Prog. Opt.* 19, 281
- Roddier F., Gilli J.M., Lund G. 1982, *J. Opt. Paris* 13, 263
- Roddier F., Léna P. 1984a, *J. Opt. Paris* 15, 363
- Roddier F., Léna P. 1984b, *J. Opt. Paris* 15, 171
- Rousset G., Madec P.Y., Rigaut F. 1991, *Temporal analysis of turbulent wavefronts sensed by adaptative optics. Digest. Topical Meeting on Atmospheric Volume and Surface Scattering and Propagation* (Florence) 77
- Sarazin M. 1986, *ESO-VLTI site evaluation II*, Nov. 86, Proc. Second Workshop on ESO's Very Large Telescope, Venice, 29 Sept.–2 Oct. 1986
- Sarazin M., Roddier F. 1990, *A&A* 227, 294
- Stock J., Keller G. 1960, *Astronomical Seeing*, in *Stars and Stellar Systems*, eds. G.P. Kuiper, B.M. Middlehurst, Vol. 1 (Chicago University Press, Chicago) 138
- Tallon M. 1989, Thesis, Nice University, France
- Tango W.J., Twiss, R.Q. 1980, ed. E. Wolf, *Prog. Opt.* 17, 239
- Tatarski V.I. 1961, *Wave Propagation in Turbulent Medium* (Dover, New York)
- Tatarski V.I. 1971, *Effects of the Turbulent Atmosphere on Wave Propagation*, Israel Program of Scientific Translation
- Vernin J., Azouit M. 1983, *J. Opt. Paris* 14, 131
- Ziad A., Borgnino J., Martin F., Agabi A. 1993, *A&A*, in press